Journal of
Applied Crystallography
ISSN 0021-8898
Editor: **Anke R. Kaysser-Pyzalla**

Optimizing the experimental design of texture goniometry

Florian Bachmann, Helmut Schaeben and Ralf Hielscher

J. Appl. Cryst. (2012). **45**, 1173–1181

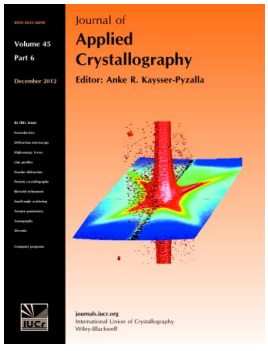

Journal of Applied Crystallography covers a wide range of crystallographic topics from the viewpoints of both techniques and theory. The journal presents papers on the application of crystallographic techniques and on the related apparatus and computer software. For many years, the *Journal of Applied Crystallography* has been the main vehicle for the publication of small-angle scattering papers and powder diffraction techniques. The journal is the primary place where crystallographic computer program information is published.

Journal of
Applied Crystallography
ISSN 0021-8898

Received 23 May 2012
Accepted 4 October 2012

Optimizing the experimental design of texture goniometry

Florian Bachmann,[a]* Helmut Schaeben[a] and Ralf Hielscher[b]

[a]Department of Geophysics and Geoinformatics, TU Bergakademie Freiberg, Germany, and [b]Applied Functional Analysis, TU Chemnitz, Germany. Correspondence e-mail: florian.bachmann@geophysik.tu-freiberg.de

Pole figure measurements with an X-ray texture goniometer equipped with a point detector are rather time consuming: depending on the angular resolution to be recorded, of the order of several hours per pole figure. Conventionally, the pole hemisphere is scanned along latitudinal small circles according to a regular grid of constant step sizes in both the azimuthal and the polar angle. In the case of sharp textures an adaptive successive local refinement strategy of the pole hemisphere may offer a better performance in less time. Then the measurement positions of the grid are highly irregularly distributed over the pole hemisphere. To avoid erratic movements when turning the specimen, the scanning order is optimized by means of resolving a travelling salesman problem such that the total travelling time is minimized. Several algorithms are described resolving the travelling salesman problem with respect to the irregular grid to be applied for each pole figure and for each step of successive refinement. A practical application to pole figure measurements exposes total savings of about 1/8 compared to the conventional scanning order. Successive local refinement of the experimental design and optimization of the order of its measurement positions are well suited to the purpose of controlling a texture goniometer.

1. Introduction

To analyse crystallographic preferred orientation it has been common practice in many laboratories to measure experimental pole intensities with an X-ray texture goniometer with a point detector. These experiments are a less costly alternative to much more involved experiments including X-ray or neutron diffraction intensities to be recorded with area detectors or electron backscatter diffraction to be recorded with an electron microscope. The major disadvantage is that it usually takes hours to measure a single pole figure depending on the required angular resolution of the pole sphere, and that usually several pole figures are required to calculate a reasonable approximation of the orientation probability density function (ODF) representing the statistical distribution of crystallographic orientations in terms of volume portions of crystallites.

Understanding that pole figures are discrete counterparts of the totally geodesic Radon transform of the orientation probability density function (Schaeben *et al.*, 2001; Bernstein & Schaeben, 2005; Bernstein *et al.*, 2009) and applying fast Fourier methods on SO(3) and $\mathbb{S}^2 \times \mathbb{S}^2$ to resolve the inverse Radon problem (Hielscher *et al.*, 2010, 2008; Hielscher & Schaeben, 2008) as encoded in the *MATLAB* (The MathWorks Inc., Natick, MA, USA) toolbox *MTEX* for texture analysis (Bachmann *et al.*, 2010), it became feasible to calculate intermediate ODFs during the actual measurements. Thus it became possible to optimize the gain of information acquired per unit time by successively adjusting the experimental design of pole figure measurements to the progress of the experiment itself. In particular, it has been suggested to successively refine an initially coarse regular spherical grid only locally where additional measurements may provide the most, essentially new information with respect to a grid of better resolution (Schaeben *et al.*, 2007). While there the focus was on the successive refinement itself and on the numerical performance of *MTEX* when processing pole intensities corresponding to a highly irregular spherical grid, here we elaborate on optimizing the scanning order to minimize the total experimental time. Since the time period to record the diffracted intensity at a specific position of the grid is user defined and constant for one experiment, only the total time needed to turn the specimen successively from one to the next measurement position through all positions of the grid can be minimized. In this way, our contribution (Schaeben *et al.*, 2007) is being completed now.

While diffraction intensities have conventionally been scanned on a regular grid according to a 'canonical' order of measurement positions along latitudinal small circles, the adaptive refinement strategy yields largely irregular, locally refined grids, where such a 'canonical' order of measurement positions may cause erratic movements of the sample stage, wasting experimental time. Thus we aim to optimize the scanning order for those locally refined grids by minimizing the total 'travelling' time taken to travel through all

measurement positions for each crystallographic form at each level of adaptive refinement. The order of measurement positions is actually optimized by solving a travelling salesman problem constrained by the constructive design of the sample stage turning the specimen. Observations justify the assumption that the time spent between two successive measurement positions depends roughly linearly on the movement of the sample stage of the texture goniometer. Then minimizing the total time of the experimental tour results in the minimum total experimental time. The successive refinement strategy itself and the optimization of the scanning order presented here are apt for step scans, whereas the counterpart of continuous scans or the use of area detectors leaves some difficulties still to be resolved. We also would like to refer the reader to our recent complementary publication (Bachmann *et al.*, 2012).

The rest of our paper is organized as follows. The problem is properly stated in §2. §3 is dedicated to approaches to resolving the travelling salesman problem. §4 provides details of an additional weighting of measurements for the numerical estimation of an ODF if the measurement positions are largely unevenly distributed on the pole sphere. An experiment applying this approach and a comparison of several numerical methods to resolve the travelling salesman problem is presented in §5. All computations have been carried out with the *MATLAB* toolbox *MTEX 3.3.0* for texture analysis. The final section provides some conclusions and perspectives.

2. Statement of problem

An ODF is usually computed from experimental pole figure intensities after a diffraction experiment with a texture goniometer has been completed. Schaeben *et al.* (2007) suggested a novel experimental strategy applying adaptive successive refinement of measurement positions in the course of the experiment. The logical steps of this procedure are summarized as follows.

Step 1: Select crystallographic forms for which pole figure intensities are to be measured.

Step 2: Define an initial experimental design as an actual grid, *i.e.* define

(*a*) an initial unique regular spherical grid or

(*b*) an initial unique spherical resolution and generate a corresponding approximately uniform grid for all crystallographic forms selected in step 1.

Step 3: Record diffraction intensities for all crystallographic forms at the positions of the actual grid.

Step 4: Estimate an intermediate ODF from all actually measured pole figure intensities, applying the inversion method of *MTEX* (Hielscher & Schaeben, 2008).

Step 5: Terminate if the refinement criteria are satisfied, *i.e.* the intermediate ODF exposes no gain of information compared to the previous refinement step or a certain angular resolution is reached; otherwise continue.

Step 6: Generate a new preliminary grid for each crystallographic form of approximately twice the spherical resolution, *i.e.* increase the preliminary number of positions to be measured by a factor of four, by intertwining additional positions in between the positions of the previous grids.

Step 7: Evaluate fitted pole figure intensities based on the intermediate ODF at the new measurement positions of the preliminary grid of each crystallographic form.

Step 8: Dismiss measurement positions of the preliminary grid where the local adaptive refinement criterion is not satisfied, *i.e.* where fitted pole figure intensities are smaller than a user-defined threshold; set the preliminary grid with the remaining measurement positions as the actual grid and continue with step 3.

The criteria to terminate in step 5 may also refer to expectation, to experience or to technical limitations of the goniometer. More involved criteria, *e.g.* evaluation of the spherical Laplacian, may be used for the actual refinement in step 6. Note that in step 6 we avoid generating new measurement positions that have already been part of the previous scan. Steps 6–8 encode the updating of the experimental design. This automated adaptive control largely reduces the total number of measurement positions and thus saves a large amount of measurement time without loss of information, especially for sharp textures (Schaeben *et al.*, 2007).

It is emphasized that the locally refined grids to be measured at each refinement step are highly irregular. Scanning these irregularly arranged measurement positions according to a random or generic sequence, *e.g.* recording diffraction intensities according to latitudinal small circles as usual, would be a large waste of experimental time in most cases. The order of the measurement positions matters, and an optimized sequence will considerably reduce the total experimental time. Since the order of measurement positions does not affect the time taken to record diffracted intensities, the optimum measurement sequence is defined such that the total time required to move the specimen is minimized. The problem to determine the optimum order of measurement positions is a travelling salesman problem (TSP), where the length of the tour is measured in terms of time, subject to constraints of the movements of the specimen due to the constructive design of the sample stage of the texture goniometer.

3. Resolving the travelling salesman problem

The objective of a TSP is to minimize the total travelling time of a salesman who travels from his starting location visiting given locations exactly once and returns back to his starting position. This problem has been well studied in operations research and provides a classical example for a notoriously NP-hard (nondeterministic in polynomial time hard) problem of combinatorial optimization.

In our application the locations are the measurement positions with respect to an actual grid, and the travelling distance of any two positions is provided by the corresponding time required to move the sample stage of the texture goniometer. Thus we analyse next the feasible movements of the sample stage, then briefly summarize common methods to

numerically resolve the TSP, and finally turn our attention to an appropriate method for our specific application to control a texture goniometer. For a more detailed introduction to and reviews of the TSP and methods of its resolution the reader is referred to the books by Gutin & Punnen (2002) and Applegate *et al.* (2011).

3.1. Implications of the sample stage: goniometer metric

Conventional X-ray diffractometers commonly use a cradle with four-circle Euler geometry to turn the specimen mounted on the sample stage. Step motors fully and automatically control the four goniometer angles $(2\theta, \omega, \varphi, \chi)$ of the cradle. The setup of the goniometer angles we refer to throughout this communication is sketched in Fig. 1. The angle $2\theta \in [0, \pi]$ usually refers to the Bragg diffraction geometry, *i.e.* the crystallographic form of a pole figure to be measured, and the angles $\omega \in [0, \pi/2]$, $\varphi \in [0, 2\pi)$ and $\chi \in [0, \pi/2]$ control the rotation of the coordinate system of the specimen relative to the coordinate system of the goniometer, *i.e.* the measurement positions in terms of specimen directions.

Let us denote by $\mathbf{x}_g$, $\mathbf{y}_g$, $\mathbf{z}_g$ the axes of the goniometer fixed coordinate system and by $\mathbf{x}_s$, $\mathbf{y}_s$, $\mathbf{z}_s$ the axes of the specimen fixed coordinate system. Then any direction $\mathbf{r}$ can be represented with respect to both coordinate systems as

$$\mathbf{r} = r_g^{(1)}\mathbf{x}_g + r_g^{(2)}\mathbf{y}_g + r_g^{(3)}\mathbf{z}_g = r_s^{(1)}\mathbf{x}_s + r_s^{(2)}\mathbf{y}_s + r_s^{(3)}\mathbf{z}_s \qquad (1)$$

by goniometer coordinates $\mathbf{r}_g = (r_g^{(1)}, r_g^{(2)}, r_g^{(3)})^\top$ and specimen coordinates $\mathbf{r}_s = (r_s^{(1)}, r_s^{(2)}, r_s^{(3)})^\top$, where the superscript $\top$ denotes the transpose. Furthermore we denote a rotation about an axis $\boldsymbol{\eta} \in \mathbb{S}^2$ through an angle γ by $\mathbf{R}_{\boldsymbol{\eta}}(\gamma) \in \mathrm{SO}(3)$.

As illustrated in Fig. 1, we assume that the X-ray beam is directed along $\mathbf{y}_g$ with respect to the coordinate system of the goniometer. A point detector is placed in the $y_g z_g$ plane of the coordinate system of the goniometer and the angle 2θ specifies the directional position of the detector to be at $\mathbf{R}_{\mathbf{x}_g}(\pi - 2\theta)\mathbf{y}_g$. Then a plane normal $\mathbf{r}_g \in \mathbb{S}^2$ in goniometer coordinates satisfies the Bragg condition for the described beam and detector positions if and only if

$$\mathbf{r}_g = \mathbf{R}_{\mathbf{x}}(\pi/2 - \theta)\mathbf{y}_g. \qquad (2)$$

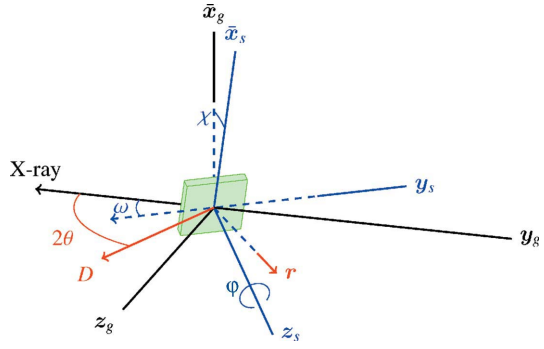

Figure 1
Experimental setup of a pole figure measurement. The black axes denote the coordinate system of the goniometer and the blue axes the coordinate system of the specimen. The sample is initially located in the $x_g y_g$ plane and the X-ray beam is directed along $\mathbf{y}_g$. A detector is positioned in the $y_g z_g$ plane at D. Then the sample is rotated about the axis $\mathbf{x}_s$ through the angle $\omega = \theta$, such that the plane normal of a crystal within the sample satisfying the Bragg condition is located at $\mathbf{r}$. Next the sample is rotated about the axis $\mathbf{y}_s$ through the angle χ and finally about the axis $\mathbf{z}_s$ through the angle φ.

The specimen is initially mounted such that the goniometer and specimen coordinate systems coincide. Then the specimen is rotated about the axis $\mathbf{x}_s$ through the angle ω first, followed by a rotation about the new axis $\mathbf{y}_s$ through the angle $\pi/2 - \chi$, and finally about the new axis $\mathbf{z}_s$ through the angle φ. Hence, the relation between goniometer coordinates $\mathbf{r}_g \in \mathbb{S}^2$ and specimen coordinates $\mathbf{r}_s \in \mathbb{S}^2$ becomes

$$\mathbf{r}_s = \mathbf{R}_{\mathbf{z}}(\varphi)\mathbf{R}_{\mathbf{y}}(\pi/2 - \chi)\mathbf{R}_{\mathbf{x}}(\omega)\mathbf{r}_g. \qquad (3)$$

Thus, we have

$$\mathbf{r}_s = \mathbf{R}_{\mathbf{z}}(\varphi)\mathbf{R}_{\mathbf{y}}(\pi/2 - \chi)\mathbf{R}_{\mathbf{x}}(\omega)\mathbf{R}_{\mathbf{x}}(\pi/2 - \theta)\mathbf{y}_g. \qquad (4)$$

It should be noted that this convention may explicitly differ for different goniometers as it depends on the constructive design of the cradle. For a different constructive design, *e.g.* the kappa geometry (Sands, 2002), goniometer angles have to be transformed into pole figure coordinates accordingly.

It is convenient to apply the Bragg–Brentano geometry and set $\omega = \theta$. Then applying the first rotation of the specimen through the angle ω causes the specimen coordinates of a plane normal $\mathbf{r}_g$ satisfying Bragg's law to be

$$\mathbf{R}_{\mathbf{x}}(\omega)\mathbf{r}_g = \mathbf{R}_{\mathbf{x}}(\theta)\mathbf{R}_{\mathbf{x}}(\pi/2 - \theta)\mathbf{y}_g = \mathbf{R}_{\mathbf{x}}(\pi/2)\mathbf{y}_g = \mathbf{z}_s = (0, 0, 1)^\top. \qquad (5)$$

Consequently, the relationship between the goniometer angles and the specimen coordinates of a plane normal satisfying Bragg's law simplifies to

$$\mathbf{r}_s = \mathbf{R}_{\mathbf{z}}(\varphi)\mathbf{R}_{\mathbf{y}}(\pi/2 - \chi)\mathbf{z}_s = (\cos\varphi\cos\chi, \sin\varphi\cos\chi, \sin\chi)^\top. \qquad (6)$$

In this way, the goniometer angles χ, φ relate directly to the polar coordinates of a pole figure. Then we only need to specify the angles χ, φ to address a measurement position of the goniometer, *i.e.* to record the diffracted intensity at the corresponding direction in a pole figure for a crystallographic form specified by 2θ and ω.

We confine ourselves to measuring each pole figure separately. Then, for each individual crystallographic form at each level of refinement, the sequence of actual measurement positions is given as an ordered list of goniometer angles (χ_i, φ_i), $i = 1, \ldots, n$, referring to the sample stage. The time required to move the specimen from one measurement position $\mathbf{r}_i = (\varphi_i, \chi_i)$ to the next $\mathbf{r}_{i+1} = (\varphi_{i+1}, \chi_{i+1})$, $i = 1, \ldots, n-1$, is uniquely determined by the speed of the step motors controlling the angles χ and φ of the cradle.

Observations justify the assumption that for step scanning the step motors controlling χ and φ move the sample stage with a speed that is a linear function of time, *i.e.* neglecting acceleration we assume that the angular velocities ω_χ and ω_φ of the step motors are constant. The bias due to acceleration could be compensated within a penalty term, as most of the acceleration usually occurs at very small movements when the

sample stage will be positioned precisely. The time $t(\mathbf{r}_i, \mathbf{r}_{i+1})$ required to move from position $\mathbf{r}_i := (\chi_i, \varphi_i)$ to position $\mathbf{r}_{i+1} := (\chi_{i+1}, \varphi_{i+1})$ is composed of the times individually required by the step motors,

$$t_\chi(\chi_i, \chi_{i+1}) = |\chi_i - \chi_{i+1}|\, \omega_\chi^{-1} + c_\chi \tag{7}$$

and

$$t_\varphi(\varphi_i, \varphi_{i+1}) = |\varphi_i - \varphi_{i+1}|\, \omega_\varphi^{-1} + c_\varphi, \tag{8}$$

where c_χ and c_φ are some constants typically required for the precise positioning of the sample stage.

If the step motors can control the tilt of the sample stage independently, then we have

$$t(\mathbf{r}_i, \mathbf{r}_{i+1}) := \max[t_\varphi(\varphi_i, \varphi_{i+1}), t_\chi(\chi_i, \chi_{i+1})]. \tag{9}$$

Generally, if we allow for simultaneous control of all four angles of the cradle, *i.e.* allowing for interchanging of crystallographic forms during the measurements, the time required to move the sample and the detector extends to

$$\begin{aligned} t(\mathbf{r}_i, \mathbf{r}_{i+1}) := \max[&t_\varphi(\varphi_i, \varphi_{i+1}), t_\chi(\chi_i, \chi_{i+1}), \\ &t_\omega(\omega_i, \omega_{i+1}), t_{2\theta}(2\theta_i, 2\theta_{i+1})], \end{aligned} \tag{10}$$

where t_ω and $t_{2\theta}$ are the times of the step motors for control of ω and 2θ accordingly. Nevertheless we avoid such experimental setups here as the size of the TSP would greatly increase.

3.2. Finding a tour

At this point it is appropriate to formulate a TSP in terms of graph theory. We call a measurement position $\mathbf{r}_i$ a node of a graph. Any two nodes $\mathbf{r}_i, \mathbf{r}_j$ of the graph are connected by an edge, and an edge is weighted by the time required to travel between those two nodes, which is here the time $t(\mathbf{r}_i, \mathbf{r}_j)$ to move the cradle analogously. The TSP amounts to the search of a permutation π of n nodes, for which we want to minimize

$$\sum_{i=1}^{n-1} t(\mathbf{r}_{\pi(i)}, \mathbf{r}_{\pi(i+1)}) + t(\mathbf{r}_{\pi(n)}, \mathbf{r}_{\pi(1)}). \tag{11}$$

The solution is called a Hamiltonian circuit, also referred to as a tour, visiting all nodes connected by edges once and only once, such that the sum of weights assigned to the edges traversed is minimum.

Finding a suitable permutation of nodes is in fact an NP-hard problem. However, the travelling time of the sample stage from one measurement position $\mathbf{r}_i$ to another $\mathbf{r}_j$ satisfies the properties of a metric TSP, namely

(*a*) $t(\mathbf{r}_i, \mathbf{r}_j) = t(\mathbf{r}_j, \mathbf{r}_i)$ (symmetry),

(*b*) $t(\mathbf{r}_i, \mathbf{r}_j) \geq 0$ (non-negativity),

(*c*) $t(\mathbf{r}_i, \mathbf{r}_j) \leq t(\mathbf{r}_i, \mathbf{r}_\ell) + t(\mathbf{r}_\ell, \mathbf{r}_j)$ (triangle inequality).

The denomination 'symmetry' indicates that there is no difference in moving from $\mathbf{r}_i$ to $\mathbf{r}_j$ or the opposite way. The designation 'triangle inequality' states that every direct movement between two measurement positions is at least as short as any indirect movement. This is worth mentioning as the solution of a metric TSP can be approximated in polynomial time with known accuracy of the solution.

Next, we give a brief review of common algorithms with special emphasis on our specific application.

3.2.1. Exact algorithms. The TSP can be formulated as a 0–1 integer programming problem. The weighted edges of the graph give rise to a system of linear equations, where the objective is to determine the edges participating in the tour by simplex methods. The integer programming formulation is still an NP-hard problem, but the TSP can be solved exactly. Recent implementations have been shown to perform well for problems of the size of 10 000–100 000 nodes (http://www.tsp.gatech.edu/concorde/benchmarks/bench99.html, http://www.tsp.gatech.edu/optimal/index.html).

Although the problem sizes of the TSPs to be resolved here are of the order of 100–10 000 nodes for each crystallographic form at each step of refinement of the automated adaptive control, exact solvers do not appeal in terms of computation times, ranging from seconds for smaller to days for larger problems. For our application it is instrumental to resolve each TSP in a reasonable time in order to minimize the total experimental time. Therefore we focus on heuristic search algorithms as already addressed by Bland & Shallcross (1989).

3.2.2. Heuristic algorithms. Heuristic algorithms can basically be distinguished in terms of tour construction and tour improvement algorithms. While the former address the problem of finding a good initial tour, the latter aim at improving a given tour. Often composite methods combining two or more heuristic procedures perform best. An heuristic tour may also serve as an initial tour for exact solvers.

Tour construction heuristics are empirically known to perform well or possess a guaranteed worst-case performance for a metric TSP.

Nearest neighbour and insertion heuristics start at an arbitrary node, and nodes not yet included in the tour are successively added at the end of the tour or inserted somewhere in the tour, such that the node added is closest to the current tour or has the cheapest tour increment. Their advantage is a complexity of $\mathcal{O}(n^2)$ or, with modifications, even of $\mathcal{O}(n \log n)$. For the cheapest insertion heuristic Rosenkrantz *et al.* (1977) showed that the tour produced is at least twice as good as the optimum tour if the problem is a metric TSP. In many practical applications these heuristics often behave quite well (Gutin & Punnen, 2002, *cf.* p. 392ff) and may be considered to initialize more sophisticated procedures for large scale problems.

MST heuristics start with the computation of a minimum spanning tree (MST). An MST is a tree containing all nodes of a graph such that each node is connected by a path and edges participating in the tree are of minimum weight. Using Kruskal's or Prim's (Cheriton & Tarjan, 1976) algorithm the computation of an MST is of numerical complexity $\mathcal{O}(n \log n)$.

The *double minimum spanning tree heuristic* is a simple heuristic proceeding as follows. In the first instance compute a minimum spanning tree of the weighted graph. Then double each edge of the tree such that all nodes of the resulting multigraph are of even degree and therefore the multigraph is Eulerian: that is, the multigraph then contains at least one cycle traversing all edges. Then traverse the multigraph and

skip nodes that have already been traversed. For instance, consider a sequence of nodes (a, b, c, b, d). Since b was traversed previously we cut short to (a, b, c, d). However, had we traversed the other way round we would have found the short cut (a, c, b, d). Although finding the least and best short cut is an NP-hard problem, skipping traversed nodes without any further considerations guarantees a resolution that is at most two times worse than the optimum tour for a metric TSP. The above-mentioned heuristic is of numerical complexity $\mathcal{O}(n \log n)$.

The *Christophides heuristic* (Christofides, 1976) is an improvement of the above procedure in the following way. Build a minimum spanning tree. Then connect all nodes of odd degree of the resulting tree by a minimum weight matching (MWM). An MWM connects every node to exactly one edge, such that the total weight of the edges is minimum. All nodes of the resulting graph are then of even degree and can be traversed as mentioned above. The tour being constructed is at most 3/2 times worse than the optimum tour. The bottleneck of this heuristic is the computation of the minimum weight matching, particularly if the total number of odd nodes is large. Using Edmond's algorithm (Edmonds & Karp, 1972) an MWM can be computed in a time proportional to $\mathcal{O}(m^4)$, where m is the number of odd edges. With more sophisticated methods the complexity can be reduced to $\mathcal{O}(m^3)$ or less (Cook & Rohe, 1999). Exploiting geometry will also considerably speed up the matching procedure. Recent implementations of the MWM problem have been tackled by Cook & Rohe (1999) and Kolmogorov (2009). Alternatively, a greedy heuristic can be employed as a compromise between numerical complexity and quality of matching. A greedy method of matching can be realized as follows. Iteratively match the remaining two closest yet unmatched nodes of odd degree. This can be done in a time proportional to $\mathcal{O}(m^2 \log m)$. Reingold & Tarjan (1981) stated that this greedy method is far from a perfect matching and is not generally appealing for a metric TSP as the total length could become twice as long as the optimum tour at most. With respect to large scale problems, we follow this approach, which has already been suggested by Bland & Shallcross (1989), who achieved sufficiently good results in their practical application.

Tour improvement heuristics attempt to optimize a given tour locally by flipping subtours of arbitrary size as long as a better resolution is feasible. Roughly speaking, whenever possible delete k edges of the actual tour and try to reconnect the heads and tails of the resulting $k+1$ segments in all possible ways, such that the new tour will be improved. With all its variations the method is referred to as the k-opt procedure and goes back to the work of Croes (1958) and Lin (1965). Considering a tour $(\mathbf{r}_1, \ldots, \mathbf{r}_i, \mathbf{r}_{i+1}, \ldots, \mathbf{r}_j, \mathbf{r}_{j+1}, \ldots, \mathbf{r}_n, \mathbf{r}_1)$ of n nodes with the two selected edges $(\mathbf{r}_i, \mathbf{r}_{i+1})$ and $(\mathbf{r}_j, \mathbf{r}_{j+1})$, the 2-opt procedure would construct a better tour if

$$t(\mathbf{r}_i, \mathbf{r}_j) + t(\mathbf{r}_{i+1}, \mathbf{r}_{j+1}) < t(\mathbf{r}_i, \mathbf{r}_{i+1}) + t(\mathbf{r}_j, \mathbf{r}_{j+1}) \qquad (12)$$

and the tour would be flipped between the nodes $\mathbf{r}_i$ and $\mathbf{r}_{j+1}$, resulting in $(\mathbf{r}_1, \ldots, \mathbf{r}_i, \mathbf{r}_j, \mathbf{r}_{j-1}, \ldots, \mathbf{r}_{i+1}, \mathbf{r}_{j+1}, \ldots, \mathbf{r}_n, \mathbf{r}_1)$. A k-opt procedure with $k > 2$ can be reduced to a sequence of 2-opt flips. We apply this kind of flip repeatedly until no gain is possible. The crucial part of the k-opt method is the search for suitable flips. It requires the computation of $\mathcal{O}(n^2)$ combinations to determine the actual best 2-opt local flip, but successively applying the actual best flip does not necessarily lead to the best possible solution. Therefore large scale problems should be tackled in a more reasonable manner. A way of speeding up the 2-opt procedure is to reduce the number of edges to be considered for a 2-opt flip operation, for instance by a tabu search excluding edges of the tour where we do not expect any tour improvement.

The heuristic proposed by Lin & Kernighan (1973) is a dynamical generalization of the k-opt procedure, focusing on finding the most promising sequence of 2-opt flips to improve the tour. The most promising 2-opt flips of the actual tour are organized in a search tree. For all flips compiled in the search tree, new most promising flips are repeatedly computed and appended till the tree has reached a convenient level of backtracking. Finally, the best branch of the search tree is chosen, which is a sequence of flips corresponding to a k-opt move. The *Lin–Kerninghan algorithm* has been widely adapted in applied mathematics, and many variations have been suggested. The chained Lin–Kerninghan heuristic additionally introduces random perturbations of the tour. They may result in more expensive intermediate tours, but the aim is to prohibit the algorithm from terminating before a better local optimum has been reached. For more comprehensive studies the reader is referred to Applegate *et al.* (2003) and Helsgaun (2000, 2009).

Table 1
List of entities involved in the numerical inversion of experimental pole figures into an orientation probability density function.

Symbol	Description
$N \in \mathbb{N}$	Total number of pole figures
$N_i \in \mathbb{N}, i = 1, \ldots, N$	Total number of specimen directions
$H_i = H(\lambda_i, \theta_i) \subset \mathbb{S}^2, i = 1, \ldots, N$	Superposed lattice planes
$\mathbf{r}_{ij} \in \mathbb{S}^2, i = 1 \ldots, N,\ j = 1, \ldots, N_i$	Specimen directions
$I_{ij} = I(\mathbf{r}_{ij}) \in \mathbb{R}_+, i = 1, \ldots, N,\ j = 1, \ldots, N_i$	Diffraction counts
$I^b_{ij} = I^b(\mathbf{r}_{ij}) \in \mathbb{R}_+, i = 1, \ldots, N,\ j = 1, \ldots, N_i$	Background intensities

4. Numerical ODF estimation revisited

Here we present an improved estimator of the unknown ODF and the unknown normalizing constants for each experimental pole figure, which is based on a statistical model [Hielscher & Schaeben, 2008, equation (16)] and a modified least-squares estimator [Hielscher & Schaeben, 2008, equations (44) and (45)].

The inventory of the problem is summarized in Table 1, where $I_i,\ I_i^b \in \mathbb{R}_+^{N_i},\ H_i \subset \mathbb{S}^2$ and $\mathbf{r}_i = (\mathbf{r}_{i1}, \ldots, \mathbf{r}_{iN_i}),\ \mathbf{r}_{ij} \in \mathbb{S}^2$, $i = 1, \ldots, N$, denote the known entities of a diffraction experiment.

The improvement concerns an adaption to very unevenly distributed measurement positions of the pole sphere by way of explicitly considering the area $v_{ij} = v(\mathbf{r}_{ij})$ of the spherical

Voronoi cell associated with the measurement position $\mathbf{r}_{ij}$ of the H_i-pole sphere, *i.e.*

$$f_{\mathrm{MLS}} = \operatorname{argmin} \sum_{i=1}^{N} \sum_{j=1}^{N_i} \left\{ v_{ij} \left[\tilde{\nu}_i(f)\, \mathcal{R}f(H_i, \mathbf{r}_{ij}) + I_{ij}^b - I_{ij} \right]^2 / I_{ij} \right\} + \lambda \, \|f\|_{\mathcal{H}} \, [\mathrm{SO}(3)]^2, \tag{13}$$

with

$$\tilde{\nu}_i(f) = \sum_{j=1}^{N_i} (I_{ij} - I_{ij}^b) \Big/ \sum_{j=1}^{N_i} \mathcal{R}f(H_i, \mathbf{r}_{ij}). \tag{14}$$

5. Numerical results

In this section we present and compare numerical results resolving the TSP for the adaptive refinement strategy. The actual diffraction experiment including successive local refinement has already been reported by Schaeben *et al.* (2007). However, optimization of the total experimental time was not an issue there. Given the successively refined grids we now resolve the corresponding TSPs numerically with the methods discussed above and thus compute tours that would have minimized the total experimental time. The travel times between two measurement positions are calculated with a model of the goniometer metric that had been fitted to experimental travel times of the same type of goniometer.

A molybdenum specimen was analysed with a Siemens Bruker D5000 diffractometer with a Huber goniometer. The measurements were successively performed for the four crystallographic forms {110}, {001}, {211} and {321}, comprising 19 190 measurement positions in total. Table 2 gives the total number of measurements of each refinement step. The initial experimental design (refinement step 0) comprised 54 measurement positions distributed equidistantly with an angular resolution of 20°. At each refinement step the angular resolution was doubled, resulting in (refinement step 1) 10°, (refinement step 2) 5°, (refinement step 3) 2.5° and finally (refinement step 4) 1.25° resolution.

We pursue five strategies to optimize the tours of measurement positions.

(1) We take the initial tour provided by the sequence of measurement positions as generated with the refinement algorithms (referred to as Direct). This tour resembles a spiral tour in latitudinal small circles from the centre to the rim of the pole figure.

(2) We apply the Christophides heuristic (Christ.).

(3) We apply the 2-opt tour improvement to the Christophides tour (Christ. 2-opt). Both algorithms have been implemented as pure functions in the *MATLAB* programming language and are distributed with the recent version of the free *MTEX 3.3.0* toolbox. The minimum weight matching of the Christophides heuristic is realized as a greedy heuristic as discussed above. For the 2-opt tour improvement we take all possible combinations into account and iteratively choose the combination with the best gain. These two implementations are anticipated to be too poor to get sufficiently close to the optimum solution of a TSP.

Table 2
Total number of measurements per crystallographic form and refinement step.

	No. at refinement step					
Crystal form	0	1	2	3	4	Total
{110}	54	46	243	778	2821	3942
{100}	54	37	154	592	3013	3850
{211}	54	69	374	1178	3480	5155
{321}	54	75	407	1342	4365	6243
Total	216	227	1178	3890	13679	19190

(4) We compare the previous implementations with the more involved chained Lin–Kernighan heuristic available with the TSP solver *Linkern*. The *Linkern* solver (http://www.tsp.gatech.edu/concorde/) is a sophisticated implementation of the chained Lin–Kernighan heuristic encoded with efficient backtracking and random perturbations by Applegate *et al.* (2003), and comes along with the *Concorde* solver (Applegate *et al.*, 1998, 2001, 2011).

(5) Another comparison concerns the *LKH* solver of the chained Lin–Kernighan heuristic. The *LKH* solver (http://www.akira.ruc.dk/~keld/research/LKH/) is another implementation of the chained Lin–Kernighan heuristic by Helsgaun (2000, 2009), which includes direct 5-opt moves and also includes an advanced tabu search.

Both TSP solvers were invoked *via* the *MTEX* toolbox within the *MATLAB* environment through the generation of a TSPLIB file (Reinelt, 1991). We applied the default settings of the programs, being well aware of the many more specifications of the possible runtime behaviour, in particular restrictions regarding the running time.

For the model of the goniometer metrics as discussed in §3.1 we used the parameters

$$\begin{aligned} \omega_\chi &= 2.45^\circ\,\mathrm{s}^{-1}, \quad c_\chi = 4.47\,\mathrm{s}, \\ \omega_\varphi &= 9.22^\circ\,\mathrm{s}^{-1}, \quad c_\varphi = 5.1\,\mathrm{s}. \end{aligned} \tag{15}$$

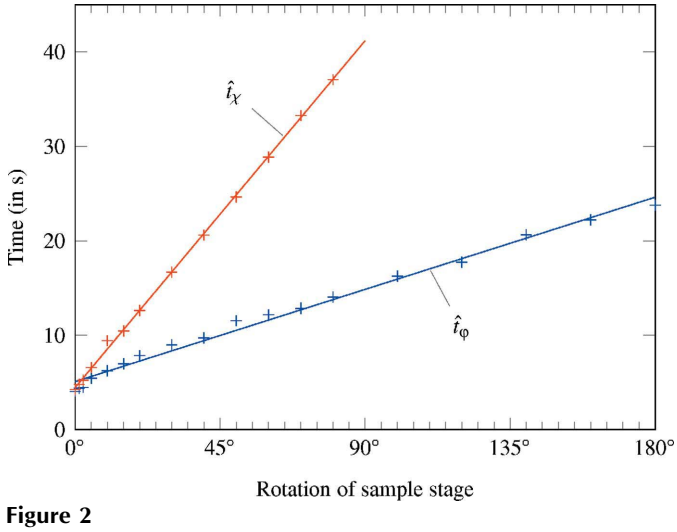

Figure 2
Required experimental time to turn the specimen for certain angular distances for the step motors moving χ (red crosses) and φ (blue crosses) and their estimated linear models $\hat{t}_\chi$ and $\hat{t}_\varphi$, respectively.

Table 3
Numerical results of pure moving time required for a measurement at each refinement step.

Step	No.	Direct	Christ.	Christ. 2-opt	*Linkern*	*LKH*
0	216	31 min 31 s	31 min 31 s	30 min 35 s	30 min 35 s	30 min 35 s
1	227	36 min 56 s	31 min 53 s	29 min 55 s	29 min 18 s	29 min 18 s
2	1178	2 h 16 min 54 s	2 h 03 min 13 s	1 h 59 min 01 s	1 h 57 min 56 s	1 h 57 min 42 s
3	3890	6 h 49 min 32 s	6 h 04 min 01 s	5 h 54 min 15 s	5 h 52 min 47 s	5 h 52 min 39 s
4	13679	22 h 10 min 15 s	19 h 59 min 02 s	19 h 48 min 58 s	19 h 46 min 49 s	19 h 46 min 23 s

Table 4
Computation time required per refinement step to resolve the TSPs.

Step	No.	Direct	Christ.	Christ. 2-opt	*Linkern*	*LKH*
0	216	<1 s	<1 s	<1 s	<1s	<1 s
1	227	<1 s	<1 s	<1 s	<1s	<1 s
2	1178	<1 s	<1 s	<1 s	1 s	10 s
3	3890	<1 s	2 s	24 s	11 s	5 min 3 s
4	13679	6 s	1 min 6 s	16 min 22 s	58 s	1 h 20 min 22 s

Table 5
Difference (%) from the best computation time and moving time for each refinement step.

Step	No.	Direct	Christ.	Christ. 2-opt	*Linkern*	*LKH*
0	216	3.08	3.08	–	0.01	0.02
1	227	26.04	8.80	2.11	–	–
2	1178	16.14	4.53	0.98	0.08	–
3	3890	16.03	3.14	0.48	–	1.34
4	13679	12.00	1.04	1.48	–	6.65

These parameters have previously been determined experimentally by random movements of the sample stage (Bachmann *et al.*, 2012). Fig. 2 shows the experimental time taken to turn the sample stage and its linear relationship. Considering 19 190 measurements, the constant time between each measurement of >4.47 s, mostly required for the precise positioning of the specimen, causes the experiment to take at least ∼24 h.

Table 3 summarizes the estimated travel times at each refinement step for the five strategies included in this comparison. The savings achieved by applying an optimized tour are about 10–25% per pole figure and refinement step, summing up to 3 h in total.

Table 4 shows the computation times required to resolve the TSP. The computations were performed on a Linux machine with an Intel Core i7 CPU 920 with 8 MB cache and 12 GB RAM running *MATLAB 2011b*. The computation time includes the time taken to generate a TSPLIB file for the solvers *Linkern* and *LKH*, for which the full weight matrix was computed. It is emphasized that there may be a general loss of computational performance when using a *MATLAB* implementation compared to a C-code implementation owing to memory access behaviour. Our 2-opt implementation is quite naive and could be improved by a more involved choice of 'kick' strategy.

Table 5 summarizes the differences of the tour lengths together with their computation time compared to the best known results, which are accomplished by *LKH* for the smaller instances and by *Linkern* for the larger ones. However, although *LKH* turned out the best tour, it required notably more time to run. It seems worthwhile to mention that the Christophides heuristic performs the better the larger the TSP. At the last refinement step the Christophides heuristic is only ∼1% off the best known solution; nevertheless applying a tour improvement heuristic is still advantageous.

Fig. 3 illustrates the process of the refinement procedure limited to the estimated travel time and the computation time for the TSPs. Further costs regarding the process are not mentioned here. A tour solution of the TSP is displayed in Fig. 4. Altogether it is a notable benefit to resolve the TSPs.

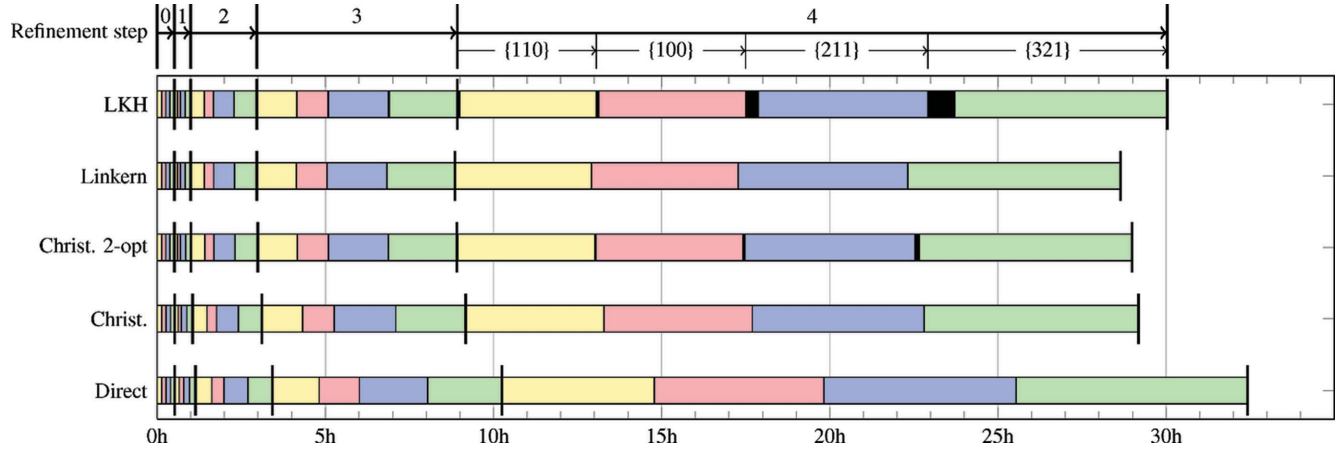

Figure 3
Cumulative estimated time (in hours) to turn the specimen for the whole refinement procedure organized by optimization method and logical order of experiment. Each coloured box denotes the pure estimated time required to turn the specimen for each crystallographic form (yellow {110}, pink {100}, blue {211} and green {321}), while the black boxes (in particular for *LKH*) denote the computation time needed to resolve the TSP corresponding to the crystallographic form. Note that *LKH* gave the best solution, but its computation time depending on its configuration negatively affects its overall performance.

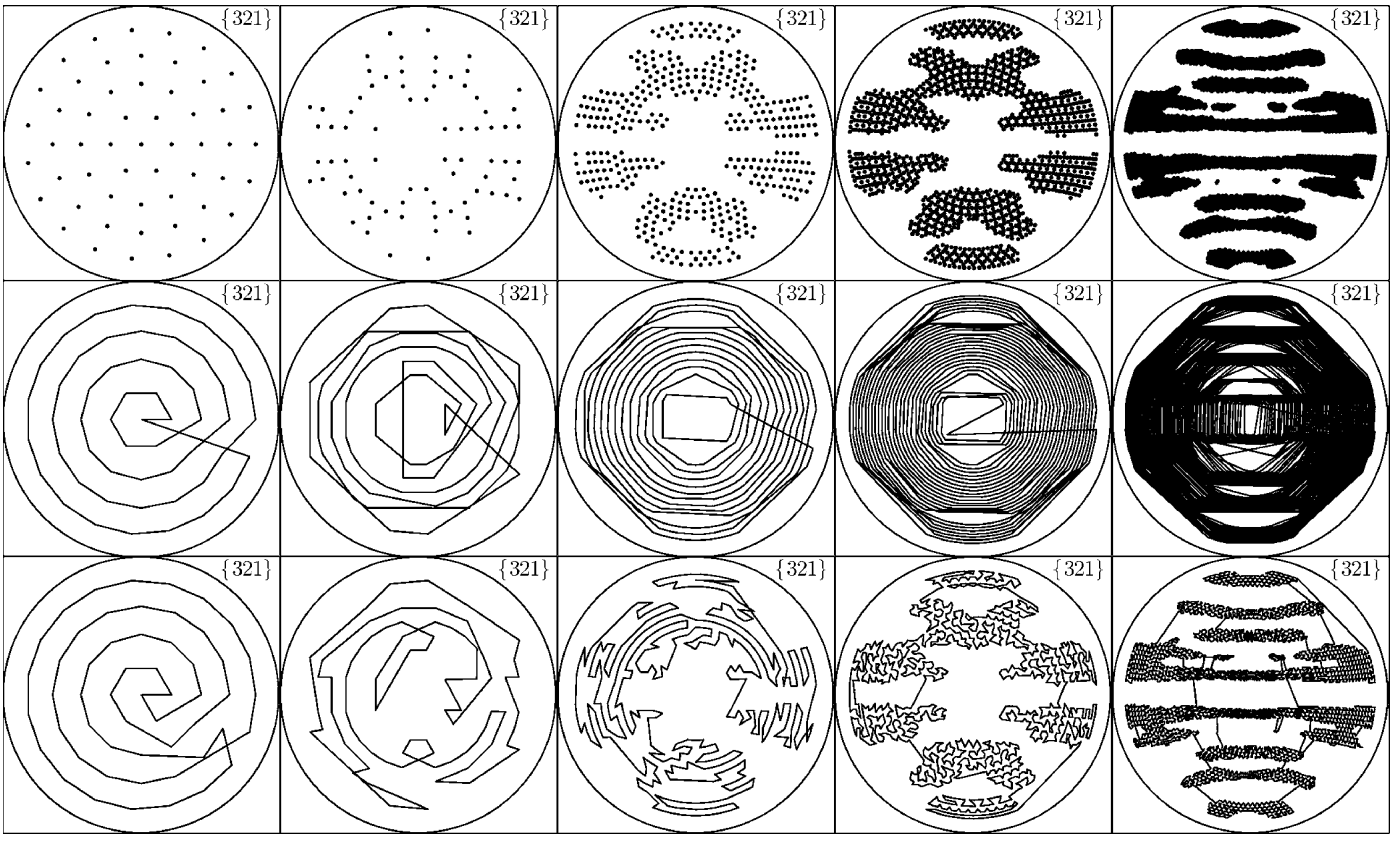

Figure 4
(Top row) Measuring positions for the initial grid and the four successively refined grids of the {321} pole figure. (Centre row) Direct measurement path without any optimization of the order of measurement positions. (Bottom row) Measuring path after solving the TSP with the Christophides 2-opt algorithm.

Detailed tables listing all measured pole figures individually and organized either by refinement step or crystallographic form are given as supplementary material.[1]

6. Conclusions

ODF-controlled successive local grid refinement provides an effective experimental design to measure diffraction pole figure intensities for the analysis of crystallographic preferred orientation. In this paper we have shown that the total experimental time can still be reduced by several hours, if the measurement positions of the largely irregular refined grids are appropriately ordered by resolving travelling salesman problems at each refinement step. Two heuristics for the resolution of the TSPs have been encoded and added to the *MATLAB* toolbox *MTEX*. They have been applied to a practical example and the results compare favourably with randomly or otherwise poorly ordered sequences. They can readily be used to control texture goniometers with point detectors.

The authors gratefully acknowledge financial funding by the German Science Foundation (DFG) (grant GO335/41-1, SCHA465/18-1). We also would like to thank the anonymous reviewers of the journal for their constructive remarks and suggestions helping us to improve the manuscript.

[1] Supplementary material discussed in this paper is available from the IUCr electronic archives (Reference: KS5321). Services for accessing these data are described at the back of the journal.

References

Applegate, D., Bixby, R., Chvátal, V. & Cook, W. (1998). *Doc. Math.* Extra Volume, §17, pp. 645–656.
Applegate, D., Bixby, R., Chvátal, V. & Cook, W. (2001). *Comput. Comb. Optim.* pp. 261–303.
Applegate, D., Bixby, R., Chvátal, V. & Cook, W. (2011). *The Traveling Salesman Problem: A Computational Study*. Princeton Series in Applied Mathematics. Princeton University Press.
Applegate, D., Cook, W. & Rohe, A. (2003). *INFORMS J. Comput.* **15**, 82–92.
Bachmann, F., Hielscher, R. & Schaeben, H. (2010). *Solid State Phenomena*, **160**, 63–68.
Bachmann, F., Witte, M., Nguyen, T., Schaeben, H. & Gottstein, G. (2012). *Acta Mater.* **60**, 4229–4234.
Bernstein, S., Hielscher, R. & Schaeben, H. (2009). *Math. Methods Appl. Sci.* **32**, 379–394.
Bernstein, S. & Schaeben, H. (2005). *Math. Methods Appl. Sci.* **28**, 1269–1289.
Bland, R. & Shallcross, D. (1989). *Oper. Res. Lett.* **8**, 125–128.
Cheriton, D. & Tarjan, R. E. (1976). *SIAM J. Comput.* **5**, 724–742.
Christofides, N. (1976). *Worst-Case Analysis of a New Heuristic for the Travelling Salesman Problem.* Technical Report, Defense Technical Information Center, Fort Belvoir, VA, USA.
Cook, W. & Rohe, A. (1999). *INFORMS J. Comput.* **11**, 138–148.

Croes, G. (1958). *Oper. Res.* pp. 791–812.
Edmonds, J. & Karp, R. M. (1972). *J. Assoc. Comput. Mach.* **19**, 248–264.
Gutin, G. & Punnen, A. (2002). *The Traveling Salesman Problem and Its Variations*, Combinatorial Optimization Vol. 12. Dortrecht: Kluwer Academic Publishers.
Helsgaun, K. (2000). *Eur. J. Oper. Res.* **126**, 106–130.
Helsgaun, K. (2009). *Math. Program. Comput.* **1**, 119–163.
Hielscher, R., Potts, D., Prestin, J., Schaeben, H. & Schmalz, M. (2008). *Inverse Probl.* **24**, 025011.
Hielscher, R., Prestin, J. & Vollrath, A. (2010). *Math. Geosci.* **42**, 773–794.
Hielscher, R. & Schaeben, H. (2008). *J. Appl. Cryst.* **41**, 1024–1037.
Kolmogorov, V. (2009). *Math. Program. Comput.* **1**, 43–67.
Lin, S. (1965). *Bell System Tech. J.* **44**, 2245–2269.
Lin, S. & Kernighan, B. (1973). *Oper. Res.* pp. 498–516.
Reinelt, G. (1991). *ORSA J. Comput.* **3**, 376–384.
Reingold, E. M. & Tarjan, R. E. (1981). *SIAM J. Comput.* **10**, 676–681.
Rosenkrantz, D., Stearns, R. & Lewis, P. (1977). *SIAM J. Comput.* **6**, 563–581.
Sands, D. (2002). *Vectors and Tensors in Crystallography*. Mineola: Dover Publications.
Schaeben, H., Hielscher, R., Fundenberger, J.-J., Potts, D. & Prestin, J. (2007). *J. Appl. Cryst.* **40**, 570–579.
Schaeben, H., Sprössig, W. & Boogaart, G. van den (2001). *Clifford Analysis and Its Applications*, edited by F. Brackx, J. S. R. Chisholm & V. Soucek, NATO Science Series II: Mathematics, Physics and Chemistry, Vol. 25, pp. 283–291. Dordrecht: Springer.